Journal of
Marine Science and Engineering

MDPI

Article

Study on Compact Pre-Swirl Duct for Slender Aft-Body Crude Oil Carrier

Jin-Gu Kang [1], Moon-Chan Kim [1,*] and Yong-Jin Shin [2]

[1] Department of Naval Architecture & Ocean Engineering, Pusan National University, Busan 46241, Korea; wind0980@naver.com
[2] Samsung Heavy Industries Co., Ltd., Daejeon 34051, Korea; prop.shin@samsung.com
* Correspondence: kmcprop@pusan.ac.kr; Tel.: +82-51-510-2401

Abstract: This study is a parametric investigation of the application of a compact type of pre-swirl duct for a slender aft-body 158k crude oil carrier. The International Maritime Organization (IMO) has created the Energy Efficiency Design Index (EEDI), which is an index related to carbon dioxide emissions, to enforce regulations on newly built ships; many solutions have been proposed, including an increase in propulsion efficiency. In the present study, a new type of energy-saving device (pre-swirl duct), the so-called ring stator, is proposed for 158k crude oil carriers, the hull form of which has been developed as a slender after-body full form to reduce the resistance by delaying separation. A conventional pre-swirl duct is no longer effective at the slender aft-body hull forms because of the small radial flow to the propeller. A parametric study was conducted through Computational Fluid Dynamics (CFD) analysis using the commercial program Star-CCM+, and an improvement of approximately 3% in the propulsion efficiency was achieved in the present study. The efficiency gain was validated through a comparison with the experimental results. The developed ring stator may become applicable to container ships through further parametric studies in the near future.

Keywords: EEDI; ESD; pre-swirl stator; CFD

check for updates

Citation: Kang, J.-G.; Kim, M.-C.; Shin, Y.-J. Study on Compact Pre-Swirl Duct for Slender Aft-Body Crude Oil Carrier. *J. Mar. Sci. Eng.* **2022**, *10*, 396. https://doi.org/10.3390/jmse10030396

Academic Editor: Md Jahir Rizvi

Received: 11 January 2022
Accepted: 21 February 2022
Published: 9 March 2022

Publisher's Note: MDPI stays neutral with regard to jurisdictional claims in published maps and institutional affiliations.

Copyright: © 2022 by the authors. Licensee MDPI, Basel, Switzerland. This article is an open access article distributed under the terms and conditions of the Creative Commons Attribution (CC BY) license (https://creativecommons.org/licenses/by/4.0/).

1. Introduction

Interest in fossil energy depletion and global warming has increased in recent years. The International Maritime Organization (IMO) has applied the Energy Efficiency Design Index (EEDI) to ships built since 2013. The EEDI represents the amount of carbon dioxide emitted during the transportation of 1 ton of cargo per mile. Emissions should be reduced by 30% by 2025, as shown in Figure 1 [1], beginning with a 10% reduction in January 2013, gradually increasing to a 50% reduction compared to 2008, and eventually leading to zero emission.

However, the EEDI does not effectively assess a realistic improvement of measures for increasing the ship operating energy efficiency, as while they can be quite effective in the considered operating point for the EEDI, their performance greatly varies in the real operating conditions [2]. For this reason, energy efficiency regulations are also being studied a lot. Ancic et al. [2] studied improving energy efficiency regulations of bulk carriers, and Ancic et al. [3] proposed the method determining environmental pollution from ships using the Index of Energy Efficiency and Environmental Eligibility (I4E). Following these efforts, the CO_2 emission regulation means that the Energy Efficiency eXisting ship Index (EEXI) will also be forced from 2023 [4]. The EEXI indicates the energy efficiency of ships during the operational phase [5]. ESDs are very effective in satisfying EEXI because it is easier to apply to existing ships.

In order to reduce the EEDI and EEXI, there are many solutions that include fuel change, renewable energy use, change of the principal dimensions of a ship, and so on. Energy-Saving Devices (ESDs) are an effective solution for decreasing the EEDI and EEXI because energy savings are simultaneously obtained without major changes to the ship

dimensions or additional expenditure. There have been many developments in ESDs. Carlton [6] categorized various ESDs into the front of the propeller (Zone I), the propeller (Zone II), and behind the propeller (Zone III), as shown in Figure 2. Each zone is named as a pre-device, main-device, and post-device. Pre-swirl stator [7] and pre-swirl duct (Mewis duct style) are the most famous pre-devices; the first is frequently used by Daewoo Shipbuilding & Marine Engineering Co. (Geoje, Korea), and recently by Samsung Heavy Industries Co. (Korea), and the second one is used by Becker Marine Systems, Hamburg, Germany [8]. CRP (Contra Rotating Propeller) [9] and Tip Rake Propeller [10] may be classified as the main device, and flexible propellers with composite materials have been actively studied not only to improve the cavitation performance but also to achieve better efficiency [11]. The post-devices comprise a Twist Rudder, Wavy Twisted Rudder [12], and Rudder-Bulb. The recently developed ESDs are shown in Figure 3.

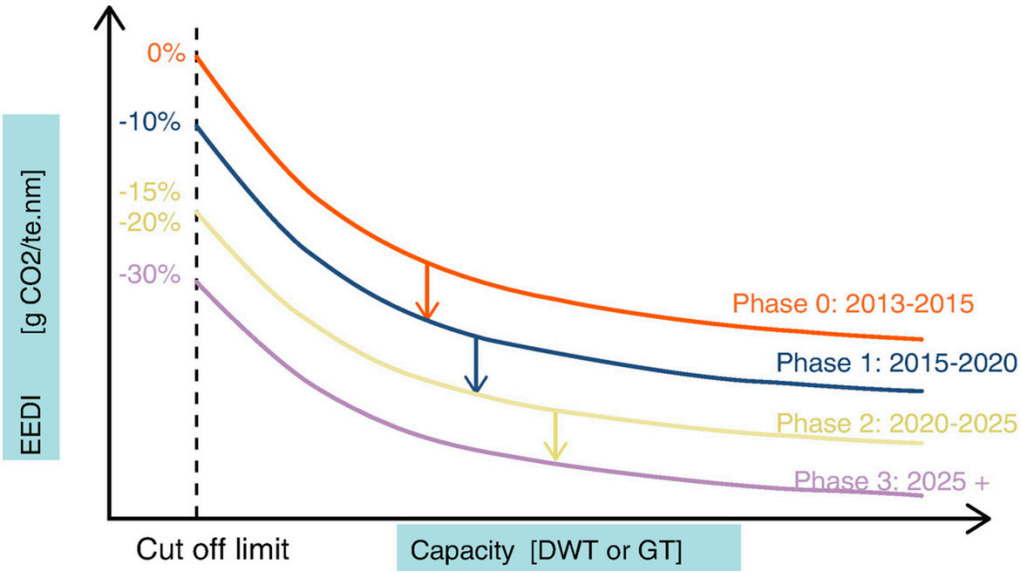


Figure 1. Phases for reduction factors of EEDI [4].

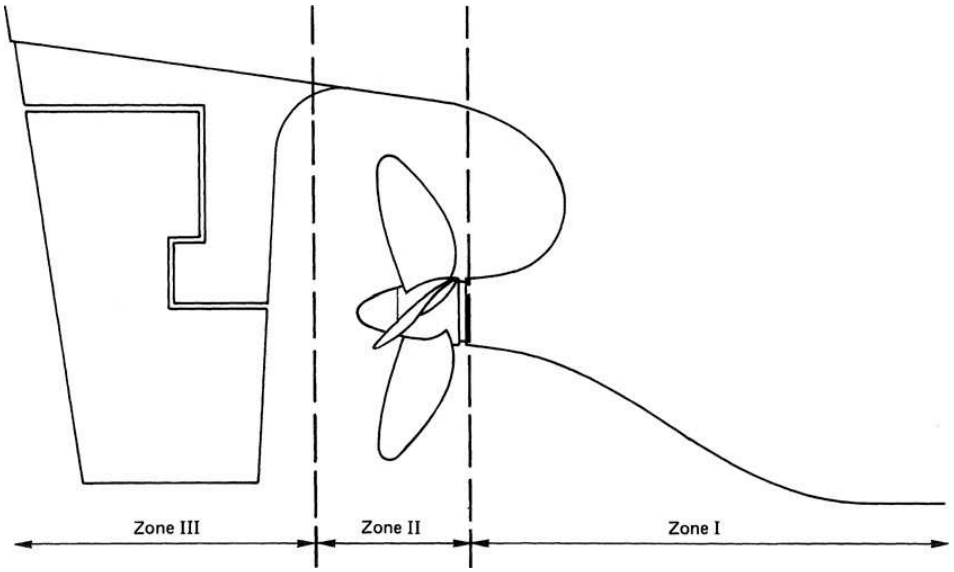


Figure 2. Classification of ESD [6]. Republished with permission from Carlton, J. S., Marine Propellers and Propulsion; published by Elsevier Science & Technology Journals, 2012.

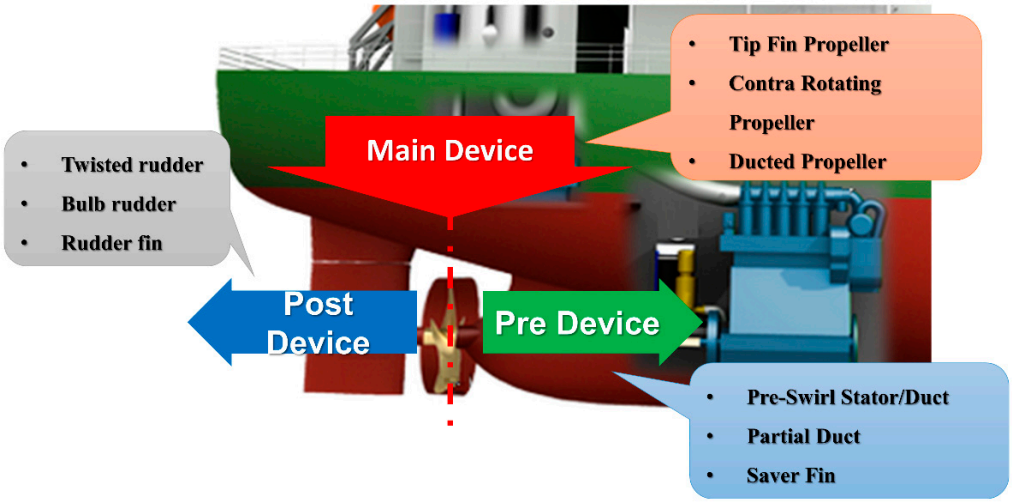


Figure 3. Recently developed ESDs at each zone.

Among these ESDs, the pre-swirl stator and pre-swirl duct seem to be the most promising ones so far. Kim et al. [7] developed an asymmetric pre-swirl stator that has better performance, efficiency, and cavitation in consideration of the upward flow of the stern body of a ship [13–15]. Koushan et al. [16] published a paper about the experimental and numerical study of PSS for chemical tanker, and Su et al. [17] studied the influence of a PSS and rudder bulb system on the propulsion performance of a large-scale ship model. Recently, the structural performance of PSS is also being actively studied. Bakica et al. [18] proposed a numerical analysis method that could predict the hydrodynamic loads and structural responses of PSS. Additionally, Vladimir et al. [19] proposed a numerical method for the vibration analysis of PSS. This device is also applicable to Liquefied Natural Gas (LNG), container ships, and slow-speed full-body ships such as tankers and bulkers.

On the other hand, the duct propeller has been adopted for the aforementioned slow-speed full-body ships for a long time. The full duct has recently been developed to be as compact as the so-called partial duct, which includes the Sumitomo Integrated Lammeren Duct (SILD) (https://nippon.zaidan.info/seikabutsu/1997/00834/contents/169.htm accessed 10 December 2021), among others, which is effective for the slender aft-body hull form [20]. This partial accelerating duct, also called the wake-equalizing duct, is also used to accelerate the slow-speed region to make the wake field more homogeneous on the propeller plane. The pre-swirl duct was successfully developed by combining the asymmetric pre-swirl stator and the partial duct by the Becker Marine System [8], as shown in Figure 4. In addition, Bakica et al. [21] analyzed the loading of circular ducts according to wave conditions through CFD.

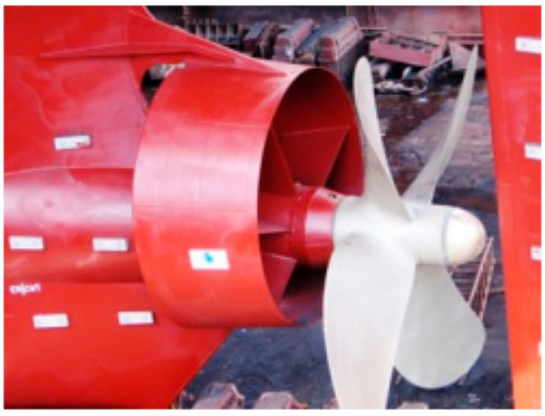


Figure 4. First installed full-scale Mewis Duct®, STARISTIND, 54,000 tdw MPC [8].

Recently, the aft-body hull form, especially slow-speed full-body, has been made slender in order to decrease the resistance by delaying separation around the stern part. Accordingly, as the aft-body hull form became slenderer, the mean wake value, which is dimensionless, has been reduced to a value little less than 0.4, which is rather similar to a container ship's wake. A more detailed description of the wake change is provided in Section 3.

The duct propeller is difficult to apply to a fast ship because of the small radial velocity. As mentioned before, the hull form of a slow-speed ship becomes slender, and the duct should be made compact because the drag of the duct becomes high. The research objective of this study is to solve the above problems. In the present study, a new type of pre-swirl duct is proposed for a slender slow-speed full-body ship, especially for the 158 K crude oil tanker. This paper contains a numerical analysis method that combines the potential theory and CFD for compact PSD design. A parametric study of the proposed compact pre-swirl duct—the so-called ring stator—was conducted for the target ship. Regarding the choice of parameter, the diameter was first chosen because that is closely related to the wake distribution, and the duct chord that is the same as the stator tip chord is also selected because the drag is proportional to the area and also the square of speed. The final parameter is the number of blades of a stator for the present parameter optimization as well as the stator pitch angle because the stator effect is not enough due to the small diameter. A more detailed description of the present optimization is described in Section 3 after the description of the numerical analysis in Section 2. The results of ring stator performance improvement were validated and presented in Section 4 through model tests at Korea Research Institute Ships and Ocean engineering (KRISO) and Pusan National University (PNU).

Regarding the scale ratio, the value of 32.8 was chosen for the validation with existing results and for the final validation test in a KRISO towing tank. A parametric study was also conducted with a scale ratio of 32.8. Due to the limitation of the PNU towing tank (L × B × D, 100 × 7 × 3.5), the scale ratio of 41.0 was used for the experiment of the final chosen design. The final test for confirmation of results has also been executed in KRISO only with the same model (λ = 41) because of budget constraints, which is a rather small model compared to the KRISO standard. In this case, the rudder has been changed for full-scale applications; therefore, an exact comparison might be limited. To determine the scale dependency, the CFD computation with the final chosen design was conducted between the scale ratios of 32.8 and 41.0 with the KRISO model test results [22].

Accordingly, as the slow-speed ship's stern part becomes slender, the present ring stator has been developed from an efficiency point of view because the conventional PSD is no longer effective for such kind of case. The ring stator is also expected to have some merits from an economic point of view, similar to the compact Propeller Boss Cap Fins (PBCFs) [23], and less structural stress burden at the stern part is another merit compared to other ESD.

2. Numerical Analysis

2.1. Potential Analysis

The design of the pre-swirl stator was conducted using the vortex-based potential analysis program PASTA developed with an in-house code. The PASTA is intended to calculate the interaction between the propeller and asymmetric pre-swirl stator in a non-uniform flow [7,13].

In general, propellers are designed to have an almost ideal angle of attack for the inflow for each radius; therefore, the lifting-surface theory is applied under the assumption of an ideal fluid in the performance analysis, and the drag force is analyzed by introducing a local resistance coefficient. However, in the case of a pre-swirl stator, a large amount of load is required to offset the propeller's rotational speed and to enable normal operation in a state that far exceeds the ideal angle of attack. Therefore, it is difficult to accurately

estimate the drag using a simple drag coefficient applied to the propeller design. The drag coefficient mentioned below is used in the design of the pre-swirl stator [13].

$$C_D = 2C_f\left[1 + \frac{t}{c} + 100\left(\frac{t}{c}\right)^4\right]\left(1 + \Delta {C_L}^2\right) + \frac{{C_L}^2}{\pi A} \quad (1)$$

Here, C_f is the resistance coefficient of the plane that varies with the Reynolds number (R_n), and ΔC_L is the difference between the total lift and lift at the ideal angle of attack. The last term considers the 3D effect, and A is the aspect ratio of the blade. In addition, c is the chord length of the 2D section of the wing, and t is the thickness. Determining the C_D using Equation (1) enables efficiency comparisons with changes in thickness, camber, and chord distributions. Adjusting the variable pre-swirl stator changes the circulation force Γ for each radius. Since Γ expresses the load applied to the blade, the performance can be compared through [24]. The PASTA program expresses Γ as an equivalent angle of attack, α_E, to enable intuitive analysis. The concept of the equivalent angle of attack is given by Equation (2). vs. represents the velocity of the ship, u is the flow velocity of the fluid entering the pre-swirl stator, c is the chord length of the 2D cross-section, and R is the radius of the pre-swirl stator.

$$\alpha_E = \sin^{-1}\left(\frac{C_L}{2\pi}\right) = \sin^{-1}\left\{\frac{2G}{\left(\frac{u}{V_S}\right)\left(\frac{c}{R}\right)}\right\} \quad (2)$$

$$G = \frac{\Gamma}{2\pi R V_S} \quad (3)$$

2.2. CFD Analysis

Regarding the coordinate system applied to the CFD analysis, the flow direction is the positive x-axis, the starboard of the ship is the positive y-axis, and the opposite direction of gravity is the positive z-axis. The commercial program Star CCM+ V. 9.04 was used for the CFD analysis. In this study, the Reynolds-Averaged Navier–Stokes (RANS) equation, considering unsteady, incompressible, and viscous flow, was used. This is expressed as follows: In the formula below, U represents the velocity of flow, p represents pressure, t represents time, ρ represents density, and μ represents the viscosity coefficient.

$$\frac{\partial U_i}{\partial x_i} = 0 \quad (4)$$

$$\rho\frac{\partial U_i}{\partial t} + \rho U_j\frac{\partial U_i}{\partial x_i} = -\frac{\partial p}{\partial x_j} + \frac{\partial}{\partial x_j}\left(\mu\frac{\partial U_i}{\partial x_j} - \rho\overline{u_i u_j}\right) \quad (5)$$

The turbulence model employed the realizable κ–ε model, and the Semi-Implicit Method for Pressure-Linked Equations (SIMPLE) algorithm was used for velocity–pressure coupling. The sliding interface moving mesh technique provided by Star CCM+ was used for the rotation flow analysis around the propeller. The Volume Of Fluid (VOF) method was used for free surface analysis. The VOF method tracks the position of the free surface, which is the boundary between the two fluids, through the volume ratio of fluids with different densities in the grid. Figure 5 shows the size and boundary conditions of the grid system for the analysis. The top, bottom, and sides of the grid area were set symmetrically, the total number of grids was approximately 3.5 million, and the grid was composed of y+ of 3–24. The computational conditions are presented in Table 1. The realizable κ–ε model was selected because several research papers in reference showed CFD results that matched well with the self-propulsion test results of PNU. CFD analysis took approximately 4 h to calculate for 1 resistance case and 1 day for 1 self-propulsion case using 184 cores of CPU (Intel_Xeon_E5-2650_v2_@_2.60GHz).

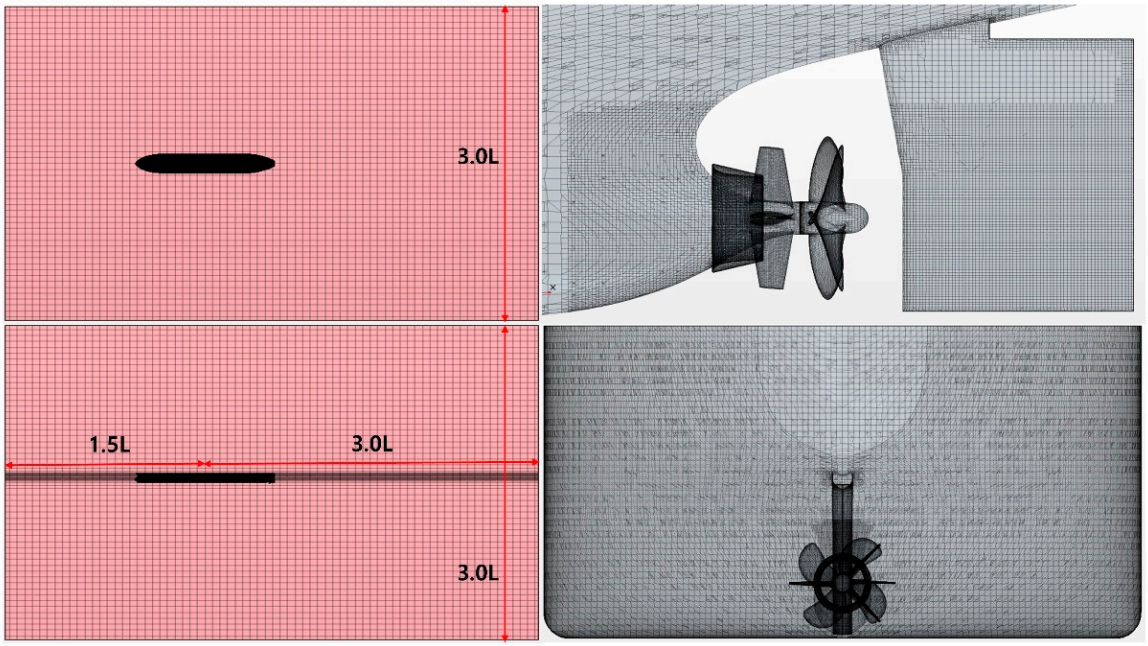


Figure 5. Grid system for CFD.

Table 1. Computational conditions for CFD.

Program	Star-CCM+ (Ver. 9.04)
Governing Equation	Incompressible RANS Equation
Discretization	Cell centered FVM
Turbulence Model	Realizable κ–ε model
Rotation Method	Sliding Mesh (Self-propulsion)
Time Step	0.01 s (Resistance), 0.003 s (Self-propulsion)
Physical Time	20 s (Resistance), 50 s (Self-propulsion)
Grid No.	Approximately 3,500,000 (Fluid region: 2.6 M, Rotating region: 0.9 M, Ring stator surface: 28,000)

2.3. Investigation of Wake and Validation

The target ship and propeller are the 158k oil carrier and KP888, as shown in Table 2 and Figure 6, respectively. The design speed and scale ratio are also 15.7 knots and 32.8, respectively.

The computed results without ESD were first compared with the experimental results for validation in a previous study [25]. A comparison of the resistance from 14 knots to 17 knots is shown in Table 3, and the self-propulsion result at a design speed of 15.7 knots is also shown in Table 4. The experiments were conducted in a KRISO towing tank. The comparison continues to a normal wake, the results of which are also similar to the experimental results, as shown in Figure 7. There is an excellent agreement in bare hull resistance between CFD and Experimental Fluid Dynamics (EFD), which is less than 0.5%, as shown in Table 2, and the hook shape and quantity of wake are also similar.

Table 2. Main dimension of target ship for scale ratio 32.8.

Scale	Length (m)	Breadth (m)	Draft (m)
Full	264	48	16
Model	8.05	1.46	0.49

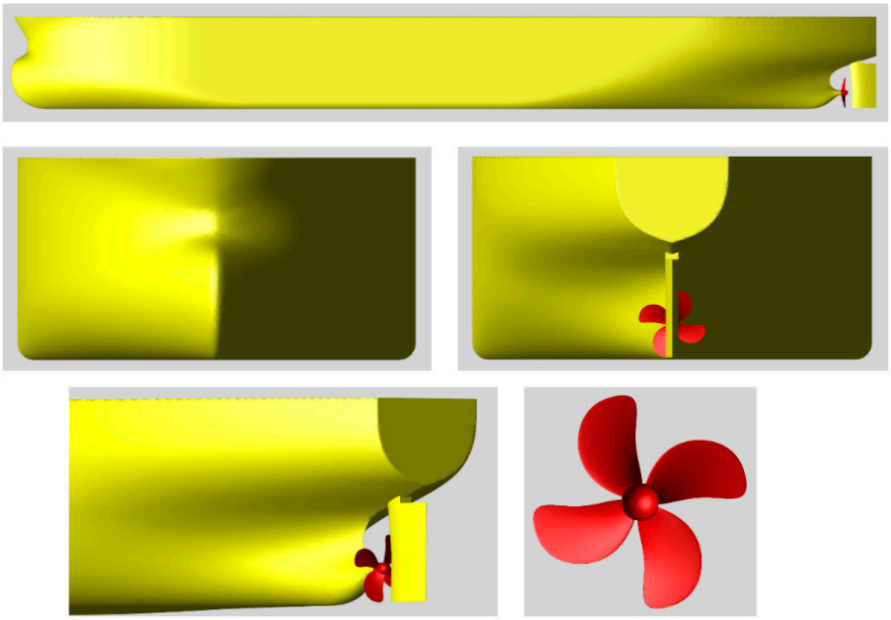


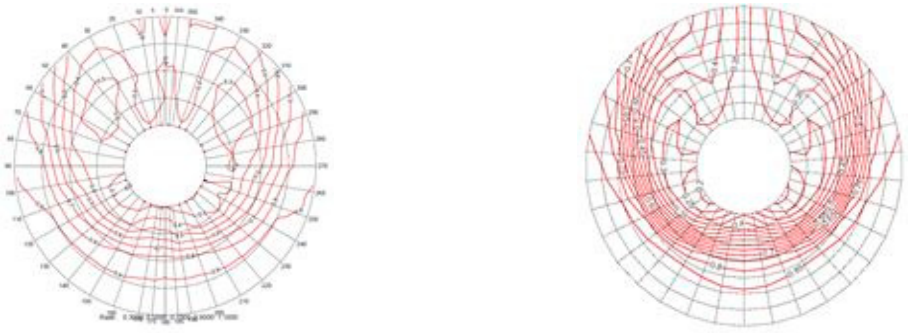
Figure 6. Configuration of target hull and propeller.

Table 3. Comparison of resistance of model-scale ship between EFD and CFD.

VS (knots)	D_EFD (N)	D_CFD (N)	Diff. (%)
14	49.93	49.95	0.04
15	56.81	57.06	0.44
15.7	62.09	62.38	0.47
16	64.47	64.68	0.33
17	72.70	72.93	0.32

Table 4. Comparison of self-propulsion analysis results between bare hull and with PSD.

	n_M (rps)	T_M (N)	Q_M (Nm)	P_D (kW)
Bare hull	7.83	41.07	1.26	592.06
With pre-swirl duct	7.52	43.58	1.29	582.39
Diff. (%)	−4.0	6.1	2.4	−1.6



(**a**) (**b**)

Figure 7. Comparison of nominal wake between EFD and CFD: (**a**) W_n = 0.452 (EFD); (**b**) W_n = 0.440 (CFD) [25].

As mentioned before, the aft-body hull form of a slow-speed ship has recently been made slender, even similar to that of container ships. This recent trend is specifically shown in Figure 8, where the tanker's mean wake becomes smaller, being less than 0.5 (the present case is 0.452) approximately 5 years ago, while the mean wake of a slow-speed full-body ship (176K bulk carrier) was 0.623 approximately 15 years ago. Recently, the mean wake has become less than 0.4, which is more similar to that of the container ship. As the stern shape becomes slender, it is difficult to apply ESD. This is because the drag generated by ESD increases and a minor radial flow makes the application of the duct difficult. According to this trend, the duct should be smaller or absent to minimize the drag of the duct.

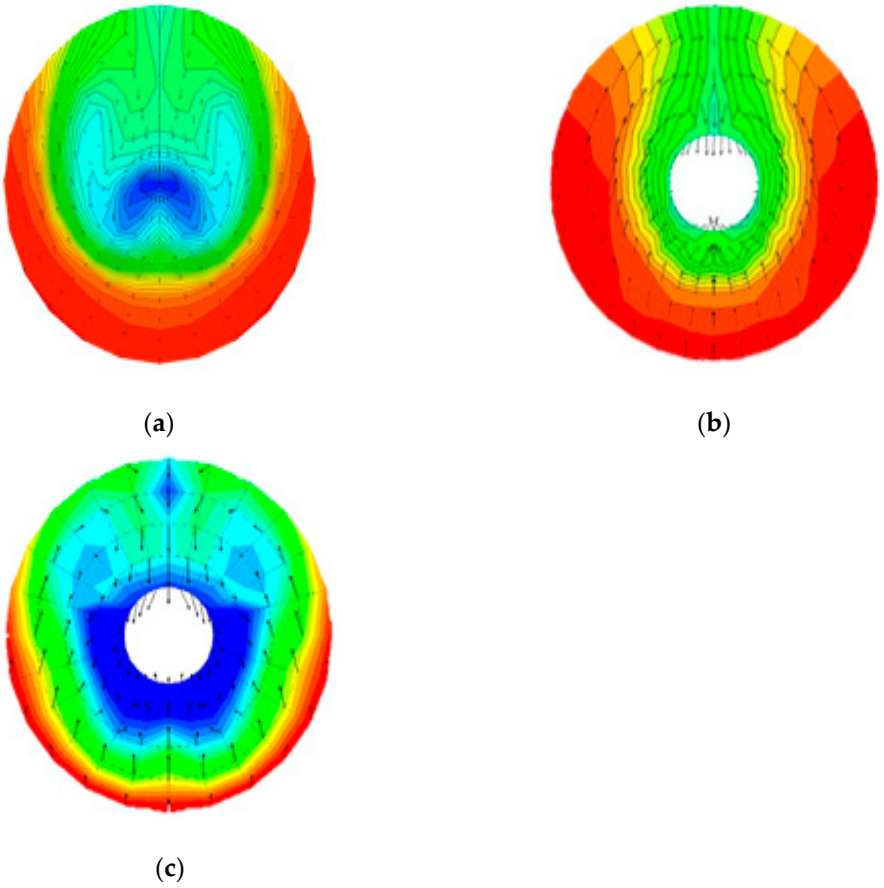


Figure 8. Comparison of nominal wake by ship types in EFD: (**a**) 158 K crude oil tanker W_n = 0.452; (**b**) KCS container ship W_n = 0.261; (**c**) 176 K bulk carrier W_n = 0.623 [25].

The developed pre-swirl duct was successfully applied to 176K bulk carriers [26]. An efficiency gain of approximately 8% was obtained using the developed PSD. The same design concept of PSD was applied to the target ship 158K crude oil tanker; however, a sufficiently satisfactory improvement in propulsion efficiency was not obtained. An improvement of only 1.6% gain in terms of delivered horsepower on the model scale was obtained, as shown in Table 4, which is quite different from previous results [26].

The purpose of the present study is to develop a new type of PSD that can increase the efficiency by more than 3% in slender aft-body hull form. To develop a compact PSD that does not cause excessive drag, a parametric study should first be conducted. In the present study, CFD computation was validated by comparison with the self-propulsion test results. The thrust and torque of the propeller were compared between EFD and CFD at a design speed of 15.7 knots by adjusting the rpm of the CFD (471.9 rpm) case to the EFD (470.4 rpm). The computed results of the thrust and torque are very similar to those of the EFD, as shown in Table 5.

Table 5. Comparison of self-propulsion analysis results between EFD and CFD.

	EFD	CFD	Diff. (%)
Self-propulsion RPM	470.4	471.9	0.3
Thrust (N)	40.4	41.7	3.1
Torque (Nm)	1.29	1.29	0.0

3. Design of Ring Stator

As shown in Figure 8, the fast region is rather wide despite the slow-speed ship's wake. The developed accelerating-type ring stator seems appropriate, particularly for this type of vessel in consideration of fitting the high wake region. This device is also advantageous in avoiding the tip vortex risk from the stator tip to the propeller and rudder. Regarding stator design, the pitch angle is the most important factor. In a previous study [24], the potential-based pitch design showed a good correlation with the experimental results. In the case of duct design, the duct angle is determined by aligning the flow direction through CFD computation [26], and NSMB Nozzle 19A was adopted for the present foil shape. A parametric study of the duct and the stator was conducted with variations in diameter, a taper ratio of a stator, length and thickness of duct, and so on. The initial reference case was first determined, and then a parametric study was carried out as mentioned before. The flow chart of the overall ring stator design is shown in Figure 9.

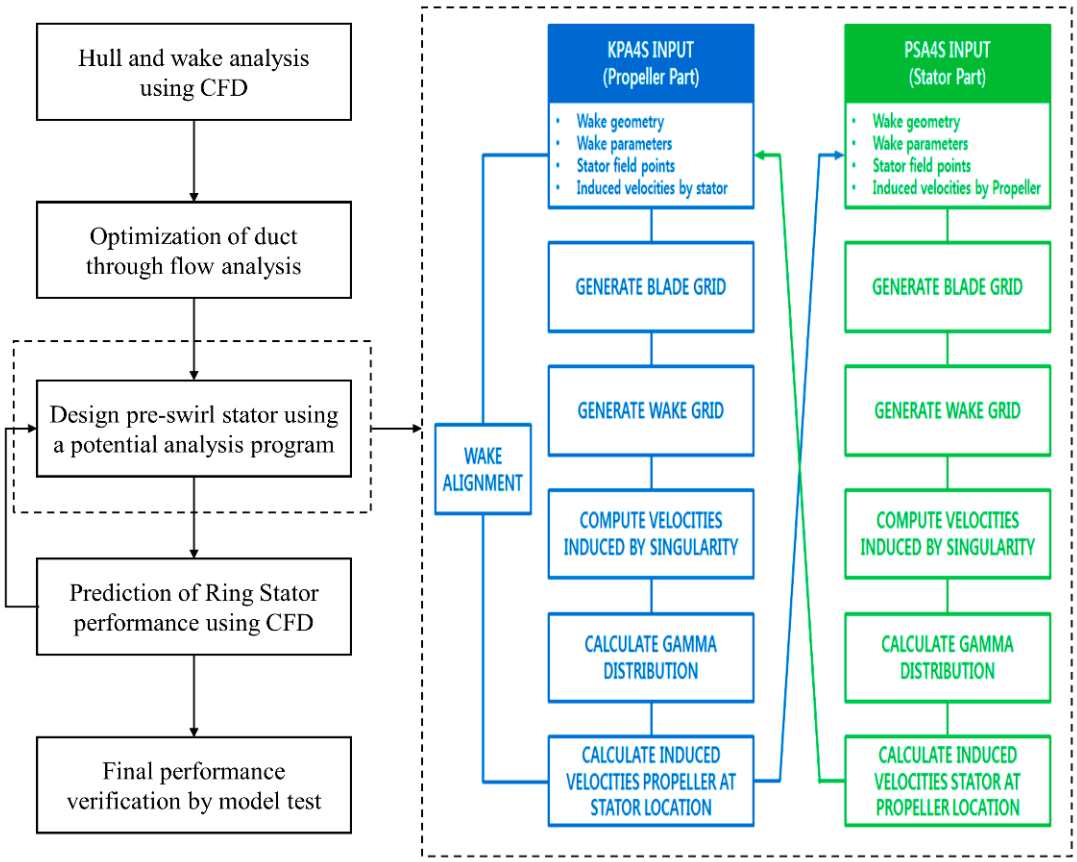


Figure 9. The flow chart of ring stator design.

3.1. Initial Reference Case

Considering the fast-flow region at the astern part, the standard diameter of stator and ring (duct) is set to be half of the propeller diameter that was decided based on the wake distribution as shown in Figure 10. Additionally, the chord and thickness of the stator are designed to be 10% less than those of the optimized corresponding values in [7], that

is, almost the minimum value in consideration of structural strength. The most important parameter of the equivalent angle was determined to be 14°, which has been proven in various previous studies [27,28]. The ring stator is longitudinally located at 0.5R of the propeller, just ahead of the propeller position. The geometry of the initial reference ring stator is listed in Table 6, and the pitch angles at each blade are listed in Table 7. The blades were numbered according to each position, as shown in Figure 11 [29].

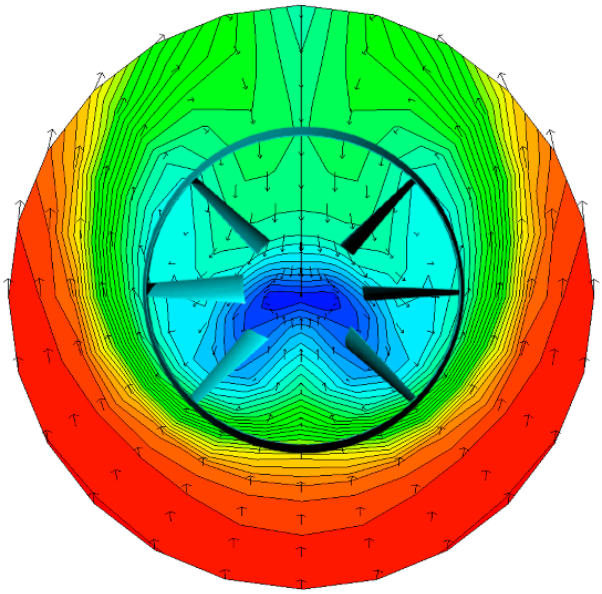


Figure 10. Determination of ring stator diameter considering wake distribution.

Table 6. Geometry of ring stator according to radius.

r/R	c/D	f/t	t/D
0.20	0.1771	−0.4088	0.0368
0.25	0.1741	−0.4052	0.0351
0.30	0.1711	−0.4013	0.0333
0.40	0.1652	−0.3919	0.0299
0.50	0.1593	−0.3801	0.0264
0.60	0.1534	−0.3648	0.0229
0.70	0.1474	−0.3439	0.0194
0.80	0.1416	−0.3142	0.0160
0.90	0.1356	−0.2676	0.0125
0.95	0.1327	−0.2331	0.0107
1.00	0.1297	−0.1853	0.0090

Table 7. Pitch angles of initial reference pre-swirl stator.

No. Blade	Position (°)	Angle (°)
1st blade	45	2
2nd blade	90	8
3rd blade	135	3
4th blade	270	2

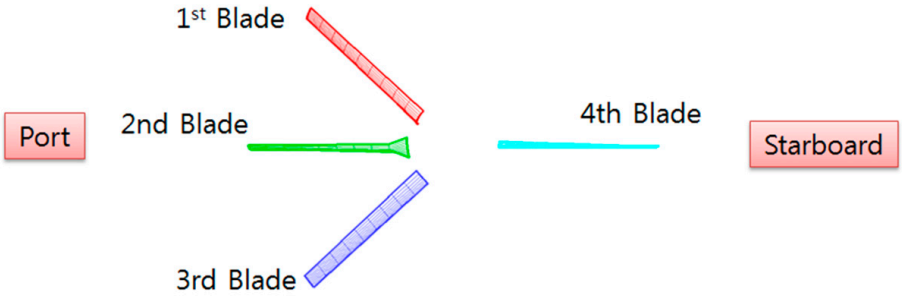


Figure 11. Blade position of each blade of pre-swirl stator.

3.2. Parametric Studies

Through Cases 2–4, the major parameters, such as the number of blades, diameter, and tip chord (same as ring chord), were varied to determine the difference in efficiency, as shown in Figure 12. After the combination of parameters was selected as Case 5, the optimum pitch angle was investigated. To confirm the previous value of 14° as the optimum equivalent angle of attack, the equivalent angles of attack were varied in the range of 12°–16°. The cases of the parametric study are listed in Table 8. The corresponding pitch angle with the equivalent angle of attack and required delivered horsepower are listed in Tables 9 and 10, respectively.

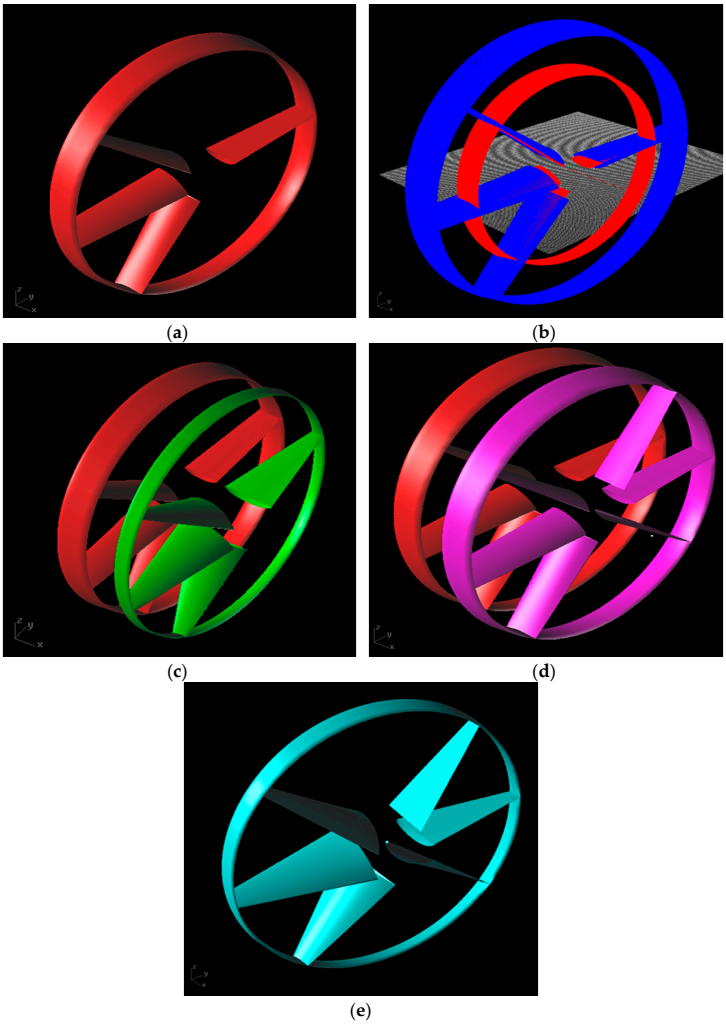


Figure 12. Configurations of parametric design of ring stator: (**a**) Case 1; (**b**) Case 2; (**c**) Case 3; (**d**) Case 4; (**e**) Case 5 [25].

Table 8. Cases of ring stator design.

NO. Case	Ring Stator
Bare hull	-
Case 1	Initial reference
Case 2	Diameter effect
Case 3	Chord effect
Case 4	Number of blades effect
Case 5	Combine (Case 3+4)
Case 6	Pitch angle effect (Eq. angle 12°)
Case 7	Pitch angle effect (Eq. angle 15°)
Case 8	Pitch angle effect (Eq. angle 16°)

Table 9. Pitch angles of Cases 6, 7, 8.

No. Blade	Case 6	Case 7	Case 8
1st blade	7	15	17
2nd blade	17	25	27
3rd blade	11	20	22
4th blade	8	16	18
5th blade	2	9	11
6th blade	4	11	13

Table 10. Comparison of delivered horsepower.

No. Case	P_D (nQ)	Diff. (%)
Bare hull	608.99	-
Case 1	602.65	−1.04
Case 2	606.38	−0.43
Case 3	600.65	−1.37
Case 4	600.85	−1.34
Case 5	598.40	−1.74
Case 6	599.21	−1.61
Case 7	588.28	−3.40
Case 8	599.23	−1.60

In Case 2, the diameter was increased up to 70% of the propeller diameter from the reference of 50% diameter of the propeller. In Case 3, the tip chord length was increased to 20% to determine the dependency on efficiency. According to the fast flow region, especially the outer region, the large-diameter, and wide-chord cases became worse, as mentioned before. The minimum chord length of the duct should be determined by considering both the structural reliability and efficiency. The chord length of the duct in this study, which is the same as the stator tip chord length, was 3% of the propeller diameter. In Case 5, symmetric six blades of the stator and asymmetric four blades were compared because the flow energy is concentrated at the center of the propeller owing to the slender hull form. Through Cases 6–8, the equivalent angle of attack was varied, and the pitch angles were designed according to each equivalent angle of attack, as shown in Table 9.

3.3. The Results of Numerical Analysis

The computational results are summarized in Table 10, where the Delivered Horse-Powers (DHPs) are compared. At the same design speed point, the DHP can be considered as the efficiency, although it is evaluated on the model scale. According to an increase in the diameter (Case 2), the efficiency became slightly worse than that in Case 1, which means that Case 2 was not beneficial because of the increase in diameter. Similarly, the efficiency of the wide chord case was worse than that of the small case (Case 3). The symmetric six blades case was slightly better than the reference. Based on the above results, six blades with a small diameter (half of the propeller diameter) and small chord length (3% of propeller diameter) were adopted. The pitch angles were finally varied to determine the optimum equivalent angle of attack, as mentioned before. An equivalent angle of attack of 15° (Case 7) was the best in terms of efficiency, as shown in Table 10. A comparison of the DHPs for all the cases is shown in Figure 13.

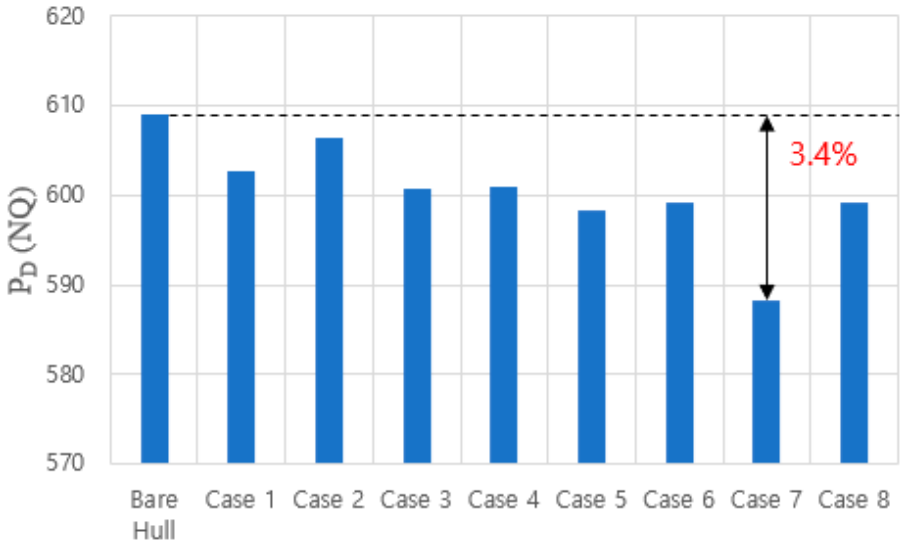


Figure 13. Comparison of the delivered horsepower of each case.

4. Results of Model Test and Discussion

To validate the present design experimentally, the bare hull and best case (Case 7) models were manufactured, and model tests were performed at the towing tank of Pusan National University in Korea. The specifications of the target ship and propeller are shown in Tables 11 and 12, and the model ship and its appendages are shown in Figures 14 and 15.

A comparison of the resistance test results between the bare hull and Case 7 at the design speed of 15.7knots is shown in Table 13. The International Towing Tank Conference (ITTC) 1957 2D method [30] was used to evaluate the performance of the full-scale resistance in order to exclude the uncertainty of form factor. It was found that as the ring acted as an accelerating duct, the Effective HorsePower (EHP) slightly decreased, even though the stator was also attached (Case 7). A comparison of the self-propulsion test results is presented in Table 14. The ITTC 1999 method [31] was used to estimate the full-scale performance, and as a result, an improvement of approximately 2.6% was achieved in terms of DHP. Moreover, when compared with the CFD results, the model test showed somewhat smaller results at the DHP. This difference might be owed to the Reynolds effect in the present compact device. In terms of the chord of the ring, the length is only 8.75 mm, that is, the local Reynolds number is approximately 1×10^4. Although the wake region seems turbulent, there might be some laminar region that causes some separation in contrast to the fully turbulent CFD computation. A more detailed investigation is required in the near future.

Table 11. Main dimension of target ship for scale ratio 41.0.

158K Crude Oil Tanker	Ship	Model
Scale Ratio	41.0	
LPP (m)	264.0	6.439
B (m)	48.0	1.171
LWL (m)	268.9	6.559
S (m^2)	18,276.9	10.863
SBK (m^2)	103.0	0.061
AT (m^2)	699.0	0.416
DISV (m^3)	165,466	2.401
KB	8.349	0.204
LCB+f (m)	9.050	0.221
LCF+f (m)	−0.140	0.003

Table 12. Main dimension of target propeller.

KP888		Propeller Dimension	
Diameter_S (m)	8.20	Chord_0.7R	0.3210
DIiameter_M (m)	0.20	Thickness_0.7R	0.0119
Expanded Area Ratio	0.576	Hub Diameter (m)	0.1700
Pitch Ratio_Mean	0.748	Rake	0
Pitch Ratio_Tip	0.759	Skew	19.85
Pitch Ratio_0.7R	0.761	Rotation Direction	Clockwise
Pitch Ratio_Root	0.655	Material	Aluminum
KP (μm)	30	Number of Blades	4
		Section Type	NACA66

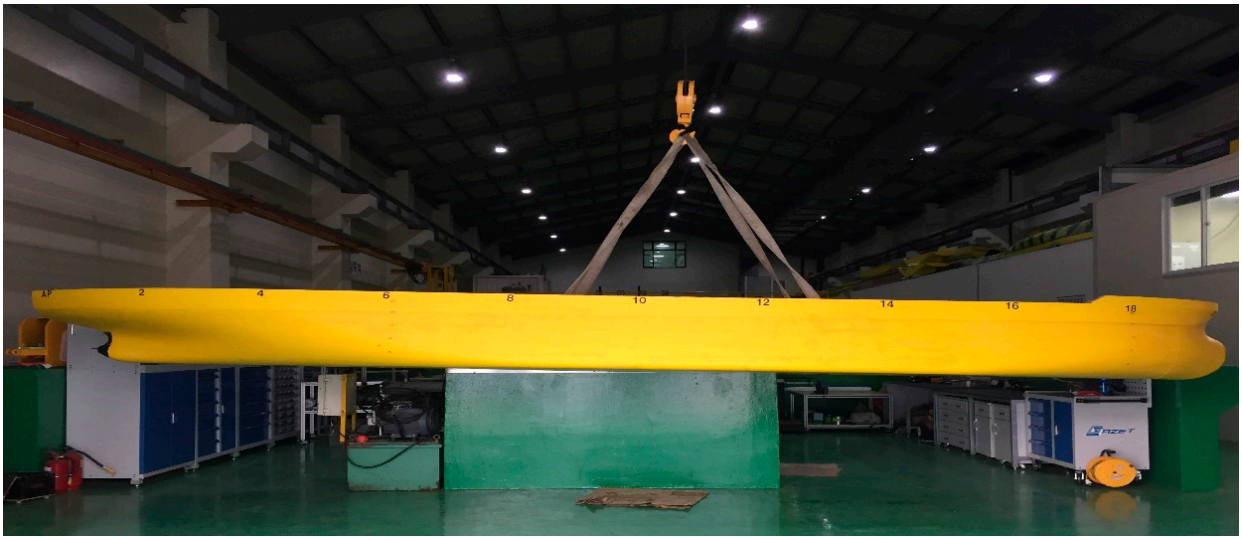


Figure 14. The model ship of 158K crude oil tanker.

To validate the scale dependency in the computation, the case of λ = 41.0 was also computed and compared with Case 7 of λ = 32.8, as shown in Table 15. There is a slightly low efficiency gain (2.85%) in the scale factor of λ = 41.0 compared to the case of λ = 32.8.



Figure 15. The model ESD of 158K crude oil tanker (Case 7).

Table 13. Results of the resistance model test.

	Bare Hull	Case 7	Diff. (%)
V_S (knots)	15.7		-
V_M (m/s)	1.261		-
RTS (kN)	1236.1	1233.5	–0.21
EHP (PS)	13,573	13,544	–0.21

Table 14. Results of the self-propulsion model test.

	Bare Hull	Case 7	Diff. (%)
V_S (knots)	15.7		-
V_M (m/s)	1.261		-
n_S (rpm)	86.63	85.73	–1.04
Thrust (N)	1571	1569	–0.13
Torque (N·m)	1619	1593	–1.61
WTM	0.4327	0.4498	3.95
WTS	0.3194	0.3365	5.35
η_D	0.680	0.696	2.35
DHP (PS)	19,970	19,450	–2.60

Table 15. Comparison of CFD results for scale dependency.

	Bare Hull	Case 7	Diff. (%)
P_D (nQ) λ = 32.8	608.99	588.28	–3.40%
P_D (nQ) λ = 41.0	289.01	280.76	–2.85%

Finally, the results of the KRISO model test were briefly introduced [22]. As mentioned before, the large-scale case was only tested for the final verification of the developed PSD. For the application of an actual full-scale ship, a bulb-type rudder was applied instead of a conventional rudder. The efficiency gain was 3.4%, which is higher than that of 2.6% in

the PNU towing tank. The rudder bulb's effect is normally at most 1–2%. Considering the bulb effect, the gain might be around 3%, which is a reasonable value between the CFD computation and model test results at the PNU.

5. Conclusions

In the present study, a new type of PSD—the so-called ring stator—was proposed for a 158 K crude oil carrier. The ring stator was designed to adapt to the wake of the propeller plane. In the case of the target ship, the stern is rather slender, even though it is a low-speed full-body ship. Therefore, in order to prevent excessive drag increase due to additives, the design was made compact so as to minimize the diameter of the ring stator and the length of the chord at the tip of the blades. A parametric study was conducted to determine the dependence of efficiency according to variations in geometry, and its performance was validated using CFD and model tests.

A parametric study was conducted by selecting the diameter, the number of blades, the taper, and the pitch angle of the stator and chord of the duct as design variables for the ring stator. The most important parameter for the present compact ring stator is diameter, which is decided based on the wake distribution. The optimally decided value of diameter is half of the propeller diameter. The duct chord that is the same as the stator tip is selected as 10% of normal PSD for the minimum drag. In the case of the number of stator blades, six is chosen to cancel out the hub vortex energy enough because the flow energy is concentrated at the center of the propeller owing to the slender hull form. Regarding the pitch angle of the stator, it is similar to the existed other stator cases.

Finally, an increase of approximately 3% (Case 7) in propulsion efficiency, compared to that without the device, was obtained by applying the best choice through CFD and validated by a model test. A comparison of the model power of $2\pi nQ$ between the model test and CFD was performed. To compare the model test results more precisely, a computation with the same scale as the model test was conducted, and the computed efficiency gain was 2.9%, which is slightly lower than that with a small-scale ratio. Finally, a 2.6% efficiency gain at the full-scale performance was obtained based on extrapolation with the model test.

There might still be room for improvement, such as in terms of the optimum attachment position of the ring stator, etc., and, regarding the full-scale performance, it is necessary to continue further research, including the performance of full-scale computation.

Author Contributions: This study is the result of collaborative teamwork. Project administration, validation, writing—original draft, writing—review and editing, J.-G.K.; conceptualization, supervision, M.-C.K.; visualization, investigation, Y.-J.S. All authors have read and agreed to the published version of the manuscript.

Funding: This study was supported by Basic Science Research Program through the National Research Foundation of Korea (NRF) funded by the Ministry of Science, ICT and Future Planning (NRF-2019R1F1A105808013).

Institutional Review Board Statement: Not applicable.

Informed Consent Statement: Not applicable.

Data Availability Statement: Not applicable.

Conflicts of Interest: The authors declare no conflict of interest.

References

1. Polakis, M.; Zachariadis, P.; Kat, J.O. The energy efficiency design index (EEDI). In *Sustainable Shipping*; Springer: Cham, Switzerland, 2019; pp. 93–135.
2. Ančić, I.; Theotokatos, G.; Vladimir, N. Towards improving energy efficiency regulations of bulk carriers. *Ocean. Eng.* **2018**, *148*, 193–201. [CrossRef]
3. Ančić, I.; Vladimir, N.; Cho, D.S. Determining environmental pollution from ships using Index of Energy Efficiency and Environmental Eligibility (I4E). *Mar. Policy* **2018**, *95*, 1–7. [CrossRef]

4. IMO MEPC 76, International Maritime Organization (IMO) Adopts Key Mandatory Measures to Reduce Ships' Carbon Intensity; Establishes Ship Rating System. 17 June 2021. Available online: https://www.imo.org/en/MediaCentre/PressBriefings/pages/MEPC76.aspx (accessed on 10 January 2022).
5. Perera, L.P.; Ventikos, N.P.; Rolfsen, S.; Oster, A. Advanced data analytics towards energy efficient and emission reduction retrofit technology integration in shipping. Presented at the 31st International Ocean and Polar Engineering Conference, Rhodes, Greece, 20–25 June 2021.
6. Carlton, J. *Marine Propellers and Propulsion*, 3rd ed.; Butterworth-Heinemann Elsevier: Oxford, UK, 2012; pp. 333–342.
7. Kim, M.C.; Chun, H.H.; Kang, Y.D. Design and experimental study on a new concept of pre-swirl stator as an efficient energy-saving device for slow speed full body ship. *Soc. Nav. Archit. Mar. Eng.* **2004**, *112*, 111–121.
8. Mewis, F.; Guiard, T. Mewis Duct®—New Developments, Solutions and Conclusions. In Proceedings of the 2nd International Symposium on Marine Propulsors, Hamburg, Germany, 15 June 2011.
9. Kim, M.C.; Song, M.S.; Kang, H.J.; Kim, D.E. A numerical and experimental procedure for the open water characteristics of contra-rotating propellers for EEDI improvement. *J. Korean Soc. Mar. Environ. Energy* **2013**, *16*, 248–254. [CrossRef]
10. Kang, J.G.; Kim, M.C.; Kim, H.U.; Shin, I.R. Study on propulsion performance by varying rake distribution at the propeller tip. *J. Mar. Sci. Eng.* **2019**, *7*, 386. [CrossRef]
11. Zodervan, G.J.; Nicola, G.; Wim, L. Hydrodynamic Design and Model Testing Techniques for Composite Ship Propellers. In Proceedings of the 5th International Symposium on Marine Propulsors, Espoo, Finland, 12 June 2017.
12. Shin, Y.J.; Kim, M.C.; Lee, J.H.; Song, M.S. A numerical and experimental study on the performance of a twisted rudder with wavy configuration. *Int. J. Nav. Archit. Ocean. Eng.* **2019**, *11*, 131–142. [CrossRef]
13. Lee, J.T.; Kim, M.C.; Suh, J.C.; Kim, S.H.; Choi, J.K. Development of a pre swirl stator-propeller system for improvement of propulsion efficiency: A symmetric stator propulsion system. *J. Soc. Nav. Archit. Korea* **1992**, *29*, 132–145.
14. Kim, M.C.; Kee, J.T.; Suh, J.C.; Kim, H.C. A study on the asymmetric pre swirl stator system. *J. Soc. Nav. Archit. Korea* **1993**, *30*, 30–44.
15. Lee, J.T.; Kim, M.C.; Van, S.H.; Kim, K.S.; Kim, H.C. Development of a pre swirl stator propulsion system for a 300K VLCC. *J. Soc. Nav. Archit. Korea* **1994**, *31*, 1–13.
16. Koushan, K.; Krasilnikov, V.; Nataletti, M.; Sileo, L.; Spence, S. Experimental and numerical study of pre-swirl stators PSS. *J. Mar. Sci. Eng.* **2020**, *8*, 47. [CrossRef]
17. Su, Y.M.; Lin, J.F.; Zhao, D.G.; Guo, C.Y.; Guo, H. Influence of a pre-swirl stator and rudder bulb system on the propulsion performance of a large-scale ship model. *Ocean. Eng.* **2020**, *218*, 108189. [CrossRef]
18. Bakica, A.; Vladimir, N.; Jasak, H.; Kim, E.S. Numerical simulations of hydrodynamics loads and structural responses of a pre-swirl stator. *Int. J. Nav. Archit. Ocean. Eng.* **2021**, *13*, 804–816. [CrossRef]
19. Vladimir, N.; Bakica, A.; Malenica, Š.; Im, H.; Senjanović, I.; Cho, D.S. Numerical method for the vibration analysis of pre-swirl stator. *Ships Offshore Struct.* **2021**, *16*, 256–265. [CrossRef]
20. Sasaki, N.; Aono, T. Energy saving device 'SLID'; Sho energy sochi 'SLID' no kaihatsu. *J. Shipbuild.* **1997**, *45*, 47–50.
21. Bakica, A.; Vladimir, N.; Gatin, I.; Jasak, H. CFD simulation of loadings on circular duct in calm water and waves. *Ships Offshore Struct.* **2020**, *15*, 110–122. [CrossRef]
22. Lee, Y.Y. *Model Test Report: BSPIS9030-11132-2*; KRISO: Daejeon, Korea, 2017.
23. Takeo, N.; Norio, I.; Hisashi, K. Energy saving technology of PBCF (Propeller Boss Cap Fins) and its evolution. *J. Jpn. Inst. Mar. Eng.* **2011**, *46*, 350–358.
24. Shin, Y.J.; Kim, M.C.; Kang, J.G.; Lee, J.H. Study on performance of asymmetric pre-swirl stator according to variations in dimensions and blade tip shape. *J. Ocean. Eng. Technol.* **2016**, *30*, 431–439. [CrossRef]
25. Kang, J.G.; Byun, T.Y.; Kim, M.C. Design and performance analysis of ring stator for crude oil carriers. *J. Korean Soc. Mar. Environ. Saf.* **2021**, *27*, 369–376. [CrossRef]
26. Song, H.J.; Kim, M.C.; Lee, W.J.; Lee, K.W.; Kim, J.H. Development of the new energy saving device for the reduction of fuel of 176k bulk carrier. *J. Soc. Nav. Archit. Korea* **2015**, *52*, 419–427. [CrossRef]
27. Lee, C.M.; Shin, Y.J.; Kim, M.C.; Choi, J.E.; Chun, H.H. Design of asymmetric pre-swirl stator for LNG carrier according to variation of stator shapes. *J. Soc. Nav. Archit. Korea* **2016**, *53*, 37–44. [CrossRef]
28. Lee, K.S.; Kim, M.C.; Shin, Y.J.; Kang, J.G. Design of asymmetric pre-swirl stator for KVLCC2 considering angle of attack in non-uniform flow fields of the stern. *J. Soc. Nav. Archit. Korea* **2019**, *56*, 352–360. [CrossRef]
29. Shin, Y.J.; Kim, M.C.; Kang, J.G.; Kim, H.U.; Shin, I.R. Validation of optimally designed stator-propeller system by EFD and CFD. *J. Brodogr.* **2019**, *70*, 133–151. [CrossRef]
30. ITTC. 1978 ITTC Performance Prediction Method. In Proceedings of the 29th ITTC, Online, 13–18 June 2021.
31. ITTC. Scaling method for ship wake fraction with pre-swirl devices. In Proceedings of the 29th ITTC, Online, 13–18 June 2021.